The effect of blade aerodynamic modelling on the prediction of high-frequency rotor airloads

Mary E. Kelly* and Richard E. Brown†
Department of Aerospace Engineering
University of Glasgow, Glasgow, G12 8QQ
mkelly@aero.gla.ac.uk, rbrown@aero.gla.ac.uk

ABSTRACT

Interactions between the blades and vortical structures within the wake of a helicopter rotor are a significant source of impulsive loading and noise, particularly in descending flight. Brown's Vorticity Transport Model has been used to investigate the influence of the fidelity of the local blade aerodynamic model on the accuracy with which the high-frequency airloads associated with blade-vortex interactions can be predicted. The Vorticity Transport Model yields a very accurate representation of the structure of the wake, and allows significant flexibility in the way that the blade loading, and hence the source of vorticity into the wake, can be represented. Two models for the local blade aerodynamics are compared. The first is a simple lifting-line model and the second is a somewhat more sophisticated lifting-chord model based on unsteady thin aerofoil theory. A marked improvement in accuracy of the predicted high-frequency airloads of the HART II rotor is obtained when the lifting-chord model for the blade aerodynamics is used instead of the lifting-line type approach. Errors in the amplitude and phase of the loading peaks are reduced and the quality of the prediction is affected to a lesser extent by the computational resolution of the wake. Indeed, the lifting-line model increasingly over-predicts the amplitude of the lift response to blade-vortex interactions as the computational grid is refined, exposing clearly the fundamental deficiencies in this commonly-used approach particularly when modelling the aerodynamic response of the blade to interactions with vortices that are much smaller than its chord. In comparison, the airloads that are predicted using the lifting-chord model are relatively insensitive to the resolution of the computation, and there are fundamental reasons to believe that properly converged numerical solutions may be attainable using this approach.

Nomenclature

a	Speed of sound
a_{ij}	Interpolation coefficients
b	Blade semi-chord
c	Blade chord, $c = 2b$
C_N	Section normal force coefficient
C_T	Rotor thrust coefficient, $T/\rho A(\Omega R)^2$
f	Reverse flow parameter
$F_j(\psi)$	Azimuthal interpolation functions
K	Coefficient of integration
M	Mach number, $M = U_\infty/a$
N_a	Number of azimuthal interpolation functions
N_r	Number of radial interpolation functions
$P_i(r)$	Radial interpolation functions
r	Blade spanwise coordinate scaled by R
R	Rotor radius
S	Local vorticity source
s	Distance in semi-chords, $s = U_\infty t/b$
t	Time
$\mathbf{u}$	Flow velocity vector
U_∞	Magnitude of the freestream velocity
w	Blade velocity relative to background flow
x	Aerofoil chordwise coordinate, $x = b\cos\varphi$
X	Rotor streamwise coordinate
Y	Rotor lateral coordinate
y_{el}	Elastic lag motion
Z	Rotor vertical coordinate
z_{el}	Elastic flap motion
$\phi(s)$	Wagner's function

*Postgraduate Research Student
†Mechan Chair of Engineering

Presented at the American Helicopter Society 65th Annual Forum, Grapevine, TX, May 27-29, 2009.

φ	Glauert's variable
Γ	Total bound circulation
λ	Velocity due to the vorticity in the flow
μ	Advance ratio
ν	Viscosity of the fluid
θ_{el}	Elastic blade torsion
ρ	Density of the fluid
τ	Unit vector parallel to blade trailing edge
ψ	Azimuth angle
$\psi(s)$	Kussner's function
ω	Vorticity in the flow
Ω	Rotational speed of the rotor

Introduction

Many of the design problems encountered by rotorcraft are directly related to the interaction between the vortices within the rotor wake and the various structural components of the aircraft. In particular, where the vortices interact with the rotating blade system, the blades are subject to highly impulsive airloads which in turn are a significant source of noise and vibration. Accurate prediction of the amplitude and position of the loading perturbations on the rotor that are induced by these blade-vortex interactions (BVIs) is known to rely critically upon two factors. These are the correct simulation of the blade deformation and the accurate characterisation of the position and strength of the vortical structures within the rotor wake. Given the current industrial focus on reduction of both maintenance costs and noise, a tool that can predict accurately the high-frequency components of the blade loading, particularly those that are responsible for the rather objectionable characteristics of the helicopter under certain flight conditions, would be of significant benefit to the designers of modern rotorcraft.

The Higher Harmonic Control Aeroacoustics Rotor Test (HART) programme (Refs. 1–4) was initiated to provide experimental insight into the structure of the rotor wake, the effect of the wake on the aerodynamic loading of the rotor blades and, thus, on the acoustic signature of the rotor. The rotor that was used in this programme was a scaled model of that used on the Bo105 helicopter. The HART II experiment was designed specifically to replicate a descending flight condition in which the loading on the rotor was known to contain significant high-frequency content due to the presence of blade vortex interactions.

Computational Fluid Dynamics (CFD) calculations of the flow around the entire rotorcraft, or even just the rotor, are extremely challenging. Nevertheless, recent advances in coupling Rotorcraft Computational Structural Dynamic (CSD) analyses to Rotorcraft CFD have demonstrated significant progress in accurately predicting the rotor blade motion and capturing the associated blade airloads. Lim *et al.* (Ref. 5) and Lim and Strawn (Ref. 6) show encouraging results in comparison to experimental data for their prediction of the BVI-induced airloads on the HART II rotor, for instance. For most CFD methods, though, the accuracy of the solution is inevitably a compromise between the need for high fidelity resolution of the wake and the computational cost that is incurred in achieving this fidelity. At present this invariably results in solutions that are grid dependent given the prohibitive computational cost of rotor calculations on grids that are sufficiently fine to resolve the detailed structure of the wake.

There is much interest, especially in the context of rotor design, in developing methods which offer high fidelity solutions but at reduced computational cost compared to full CFD calculations. Lifting-line or lifting surface type aerodynamic models have been used widely in so-called comprehensive codes to provide blade airload information. These models are generally inviscid in nature and so the wake produced by the blades is modelled separately in terms of the trailed and shed vorticity from the blades. Additional considerations are required to account for compressibility effects and stall. Such models are relatively simple and easy to implement, but the physical accuracy of their portrayal of the dynamics of the wake, especially if based on a prescribed- or free-wake approach, can be called into question especially in terms of resolving the detail of the close blade-wake encounters associated with BVI. It is often not clear whether discrepancies in the wake model, or instead in the blade aerodynamic model that lies at the source of the wake, are responsible for the deficiencies in prediction of the BVI-induced loads that appear to be characteristic of this type of approach.

The Vorticity Transport Model (VTM) is a comprehensive rotorcraft model in which the evolution of the wake is based on a time-dependent vorticity-velocity formulation of the Navier-Stokes equations, solved computationally on a structured grid system surrounding the rotor. This approach yields a very accurate representation of the structure of the wake, yet allows significant flexibility in the way that the source of vorticity into the wake can be generated. For instance, a simple lifting-line model for the blade aerodynamics can be used, or a full, primitive-variable CFD calculation of the blade flow can be embedded in the calculation (Ref. 7). This flexibility makes the VTM ideal for studying the effect of the blade aerodynamic model on the fidelity of the prediction of the high-frequency, BVI-induced loads on the rotor.

The VTM framework has been used previously to

predict the geometry of the wake system and the resultant rotor blade loading for the HART II rotor using a lifting-line model for the blade aerodynamics (Ref. 8, 9). These earlier investigations suggested that accurate prediction of the high-harmonic, BVI-induced component of the airloads on the rotor is greatly influenced by the accuracy to which the wake geometry can be represented, and also revealed that the high-frequency, BVI-induced component of the loading is very sensitive to the cell size that is used in the computations.

Nevertheless, comparisons of the predicted wake structure and the trajectory of the vortices as they pass through the rotor disc showed excellent agreement with the vortex core positions as measured during the HART II experiment. These works suggested thus that the deficiencies within the airload prediction, particularly the over-prediction in amplitude of the BVI-loading peaks at high computational resolution, were not simply the consequence of the simulations under-resolving the flow, but in fact were more likely due to an inherent mis-representation of the aerodynamic response of the blade when subjected to the very localised perturbations in its aerodynamic environment that are associated with BVI events. Indeed, the use of a lifting-line type approach where the blade chord is approximately eight times the cell size, as was the case in the most finely-resolved calculations presented in Ref. 9, stretches somewhat the assumptions that are inherent within the lifting-line model.

This hypothesis is tested in this paper by comparing the wake structure and the resultant airloads on the HART II rotor to the predictions of Brown's Vorticity Transport Model (VTM) when using two different approaches to modelling the local aerodynamics of the blades.

The first blade aerodynamic model is relatively simple and is based on an extension of the Weissinger-L formulation of lifting-line theory. In this model the strength of a bound vortex, attached to the quarter chord of the blade, is determined by enforcing a zero through-flow boundary condition at one discrete point, located at the three-quarter chord of the airfoil. Results obtained using this approach are contrasted with the results obtained using a more sophisticated blade aerodynamics model. This model is based on an extension of classical unsteady thin-airfoil theory and uses Peters's state-space formulation for the blade airloads (Ref. 10). In this so-called 'lifting-chord' approach, the aerodynamic environment of the blade is represented via a series of integrals over the chord of the blade, thus yielding a higher-order approximation to the aerodynamic loading on the blade than is given by lifting-line theory.

The dynamics of the blades in the simulations described in this paper have been prescribed to follow the experimentally-measured structural deformations of the system. This approach allows any effects on the quality of the simulation that are due to mis-representation the blade dynamics to be separated from those that are induced by the aerodynamics of the system.

Computational model

The present formulation of the Vorticity Transport Model (VTM), developed by Brown and Line (Refs. 11 and 12) couples a model for the aerodynamics of the blade to an Eulerian representation of the dynamics of the vorticity in the flow field.

The vorticity in the flow field is evolved by solution of the Navier-Stokes equations in vorticity-velocity form on a structured Cartesian grid surrounding the rotor. Assuming incompressible flow with velocity $\mathbf{u}$, the associated vorticity distribution $\omega = \nabla \times \mathbf{u}$ evolves according to the unsteady vorticity transport equation

$$\frac{\partial}{\partial t}\omega + \mathbf{u} \cdot \nabla\omega - \omega \cdot \nabla\mathbf{u} = S + \nu\nabla^2\omega \qquad (1)$$

where ν is the viscosity of the fluid. In this formulation the vorticity then becomes the conserved variable within the flow and thus is not affected by the numerical dissipation which is inherent in CFD codes based on a pressure-velocity formulation of the Navier-Stokes equations. In addition, the local rate of numerical *diffusion* is controlled very effectively by using a set of highly compressive flux limiters within the particular implementation of Toro's Weighted Average Flux method (Ref. 13) that is used within the code to convect the solution through time. At each time step, the velocity at the cell faces is obtained from the vorticity distribution using a fast multipole technique to invert the differential form of the Biot-Savart equation

$$\nabla^2\mathbf{u} = -\nabla \times \omega. \qquad (2)$$

A semi-Lagrangian adaptive grid is used to track the evolving vorticity in such a way that cells only exist in regions of the computational domain where the vorticity is non-zero. As the vorticity moves to a new location, new cells are created and any cells that no longer contain vorticity are destroyed. Thus, the grid structure is free to follow the evolution of the wake, eliminating the requirement for explicit numerical boundary conditions at the edge of the computational domain and increasing the computational efficiency of the method. Moreover, a nested grid system allows for fine resolution close to the rotor and then a systematic decrease in resolution with distance from the rotor hub.

Two separate blade models have been incorporated within this VTM framework in order to yield the aerodynamic loading on the blades. Firstly, an extension of the Weissinger-L formulation of lifting-line theory is implemented on a series of discrete panels along the length of each rotor blade. A bound vortex is attached to the quarter-chord of each panel. The strength of the bound vorticity along the length of the blade is then determined by enforcing, simultaneously, a condition of zero through-flow at the set of collocation points that are located at the three-quarter chord of each panel.

A second model for the blade aerodynamics is based on an extension of classical unsteady thin aerofoil theory and uses a particular formulation for the airloads which is based on that developed in state-space form for flexible aerofoils by Peters *et al* (Ref. 10).

The zero through-flow boundary condition allows the total bound circulation on the aerofoil to be written as

$$\Gamma = 2\pi b \left[f\left(w_0 - \lambda_0\right) + \frac{1}{2}\left(w_1 - \lambda_1\right) \right], \qquad (3)$$

where f is a reverse flow parameter designed to enforce the Kutta condition at the downwind edge of the aerofoil. The circulation is defined in terms of the weighted integrals, given by

$$\lambda_n = \frac{1}{K_n} \int_0^\pi \lambda \cos^n \varphi \; d\varphi \qquad (4)$$

and

$$w_n = \frac{1}{K_n} \int_0^\pi w \cos^n \varphi \; d\varphi, \qquad (5)$$

where w is the component, normal to the blade chord, of the blade velocity relative to the uniform background flow and λ is the component, again normal to the blade chord, of the velocity due to all vorticity in the computational domain except that which is bound to the panel under consideration. Glauert's variable φ is defined such that

$$\begin{gathered} x = b\cos\varphi \qquad (6) \\ -b \le x \le +b, \quad 0 \le \varphi \le \pi. \end{gathered}$$

and

$$K_n = \int_0^\pi \cos^n \varphi \; d\varphi \qquad (7)$$

These integrals are evaluated numerically after evaluating the integrands at several discrete points along the chord of each blade panel. In all cases described in this paper these points were cosine-distributed along the chord to give enhanced resolution of the steep loading gradient near the leading edge of the blade.

The sectional lift (per unit span) is then given by (Ref. 10)

$$L_0 = \rho U_\infty \left(\Gamma + \frac{1}{2}\lambda_1 \right) + \pi\rho b^2 \left(\dot{w}_0 \right). \qquad (8)$$

In both aerodynamic models, the trailed and shed vorticity from each vortex panel is added to the near wake downstream of the blade as the local vorticity source

$$S = -\tau \frac{\partial \Gamma}{\partial t} + \mathbf{u}_b \frac{\partial \Gamma}{\partial r}, \qquad (9)$$

where τ is the unit vector parallel to the trailing edge of the blade and $\mathbf{u}_b$ is the velocity of the trailing edge relative to the air. Most importantly in the present context, the shed vorticity distribution behind the blade is fully resolved using this approach. Its influence on the unsteady aerodynamic response of the system is thus captured directly in the simulations without the need to resort to empirical modelling of the indicial response of the blade, as is done in some comprehensive codes in order to compensate for their under-resolution or even omission in some cases of the sheet of vorticity that is shed into the flow immediately behind the blades.

The two-dimensional aerodynamic characteristics of the rotor blade sections are specified in a look-up table as a function of angle of attack and Mach number for a given Reynolds number. These characteristics can be used to precondition the zero through-flow boundary condition to allow the blade aerodynamic calculation to match closely the sectional aerodynamic characteristics, including stall, of the actual blade. As this approach is still essentially inviscid, the profile drag of the blade is calculated as a separate function of local angle of attack and is then added to the local aerodynamic force that is calculated from the blade aerodynamic model.

Fuselages or other solid bodies are represented using an unsteady vortex panel method, as described in Ref. 14. The surface of any body immersed in the flow field is discretised into a system of panels, such that each panel edge is represented as a vortex filament with constant strength, forming a closed loop of vorticity. The velocity at the centroid of any panel is calculated as the sum of the influences from all vortex filaments on the body together with the velocity induced by all the other vorticity within the flow. To determine the strengths of the vortex loops, a boundary condition of zero through-flow is enforced simultaneously at the centroids of all panels. Where present in the simulations described in this paper, the drive housing for the HART II rotor was modelled using 1908 panels. This yields a level of resolution that is comparable to previous simulations using this approach, for example as described in Ref. 14.

In the particular version of the model used in the present investigation, the motion of the blades is prescribed, based on a variable-separable interpolation of the blade deformations that were measured at discrete azimuthal and radial locations on each blade during the HART II experiment. The blade deformation was measured using a non-intrusive optical method, called Stereo Pattern Recognition, as described in Refs. 15–17.

Each component D of the blade deformation is reconstructed in the simulations by using interpolating functions of the form

$$D(r,\psi) = \sum_{i=1}^{N_r} \sum_{j=1}^{N_a} a_{ij} P_i(r) F_j(\psi), \tag{10}$$

where N_r and N_a are respectively the number of radial and azimuthal interpolation functions $P_i(r)$ and $F_j(\psi)$ used to describe the particular component of the blade deflection. The radial interpolation functions were taken to be polynomials and the azimuthal interpolation functions were taken to be the components of a Fourier series so that

$$P_i(r) = r^{(i-1)} \tag{11}$$

and

$$F_j(\psi) = \begin{array}{cc} \cos\frac{j-1}{2}\psi & \text{if} \quad j \in \{1,3,5,\ldots\} \\ \sin\frac{j}{2}\psi & \text{if} \quad j \in \{2,4,6,\ldots\}. \end{array} \tag{12}$$

The coefficients a_{ij} of the interpolation function were calculated by enforcing a simple least squares fit to the measured data for the blade deformations. This method interpolates over the relatively sparse experimental data as well as fills any gaps in the data where the markers used in the measurements could not be viewed because they lay within the shadow of the drive enclosure and the mounting support, or had peeled off the blades. The sets of coefficients that give the best approximation to the elastic flap, lag and torsional deformations z_{el}, y_{el} and θ_{el} of the blades using six radial and nine azimuthal interpolation functions are given in Ref. 8 for the HART II baseline, minimum vibration and minimum noise test cases.

The difference between the interpolation and the experimental data set for each of the measured components of the elastic deformation of the blades was within the stated error bounds on the measurements of $\pm 0.5^\circ$ for the elastic torsion and ± 0.5mm for the flap and lag deflections. Nevertheless, the reliability of the interpolation may be questioned in areas where the experimental data was particularly sparse, as was for instance the case around 0° and 180° azimuth.

Airload predictions

Rotorcraft operate in an extremely complex aerodynamic environment and, as a result, the rotor is subjected to a velocity field which is highly non-uniform. In such an environment, it is particularly important that the model that is used for the aerodynamics of the blade is able to distinguish between the effects on the blade airload which arise from an instantaneous change in angle of attack and the effects which are due to a vertical gust velocity normal to the blade.

The ability of each of the two blade aerodynamic models to distinguish between these two phenomena was ascertained by comparing their predicted response to the analytical solutions to Wagner's and Küssner's

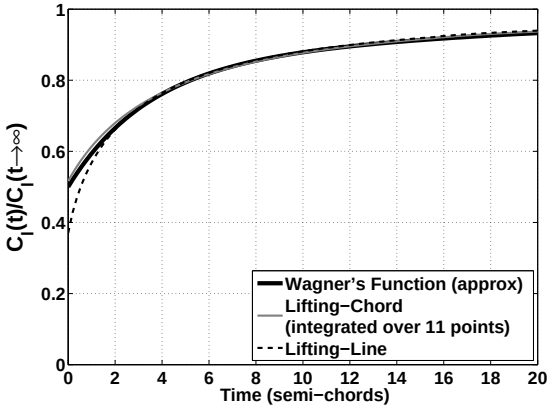

(a) *Analytical and numerical solutions compared*

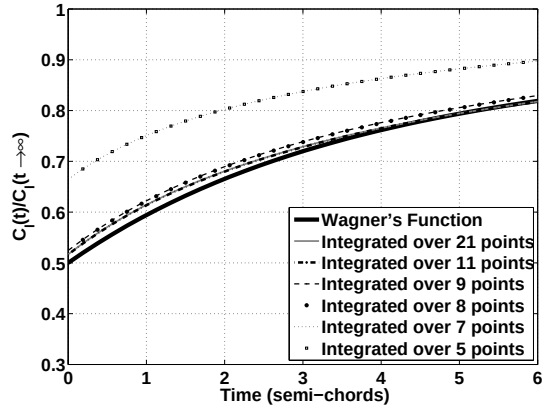

(b) *Convergence of the lifting-chord model to the exact solution as the number of points is increased over which the lifting-chord integrals are evaluated*

Figure 1: *Wagner's problem for the aerodynamic response of an aerofoil to a step change in angle of attack at time* $t = 0$.

classical problems from the field of linearized, unsteady aerofoil aerodynamics.

Wagner's Problem

Wagner's problem (Ref. 18) considers the transient lift response of a thin aerofoil of chord $2b$ to a step change in angle of attack (from zero to some small, but finite value at time $t = 0$). Wagner showed that the lift response due to circulation

$$\frac{C_l(t)}{C_l(t \to \infty)} = \phi(s) \tag{13}$$

where Wagner's function ϕ is dependent on $s = U_\infty t/b$ i.e. the number of semi-chords travelled by the aerofoil in time t. Wagner's function has an initial value of one half and asymptotes to unity as time goes to infinity.

The lift response of an aerofoil (modelled as rotor blade with a very large aspect ratio) to a step change in angle of attack, as predicted using the lifting-line model and the lifting-chord model, is compared to Wagner's analytical result* in Fig. 1(a).

This figure shows that the initial lift predicted by the lifting-line model is equal to one third of steady state lift rather than one half of the steady state value, whereas the lifting-chord approach reproduces Wagner's exact solution more accurately. Increasing the number of chordwise points that is used to numerically evaluate the weighted integrals increases the accuracy of the initial lift response of the lifting-chord model near $s = 0$. Indeed, Figure 1(b) shows the lifting-chord solution to effectively converge onto the analytical solution if the integrals are evaluated using eleven or more points distributed along the chord of the aerofoil.

Küssner's Problem

In contrast to Wagner's problem, Küssner's problem (Ref. 19) considers the response of an aerofoil to a transient change in angle of attack as the aerofoil enters and progresses through a sharp-edged, vertical gust. The transient lift response can be written as

$$\frac{C_l(t)}{C_l(t \to \infty)} = \psi(s) \tag{14}$$

where $\psi(s)$ is Küssner's function. Küssner's function has an initial value of zero and asymptotes to unity as time goes to infinity.

The aerodynamic response of an aerofoil to its progression through a sharp-edged gust, as predicted using the lifting-line model and the lifting-chord model, is compared to Küssner's analytical solution in Fig. 2.

*actually Jones's indicial approximation thereto

The lifting-chord approach captures Küssner's analytical result correctly in the sense that the response to the gust starts as soon as the leading edge of the aerofoil penetrates the gust. In contrast, in the lifting-line case, the blade does not respond until the forward edge of the gust reaches the three-quarter chord of the aerofoil, in other words the point at which the zero through-flow boundary condition is evaluated.

Interaction with an isolated vortex

Fig. 3 shows the predicted response of an aerofoil (again modelled as isolated blade with a very large aspect ratio) to an encounter with an isolated vortex. In the example shown in the figure, the vortex passes $0.25c$ below the chord-line of the aerofoil while con-

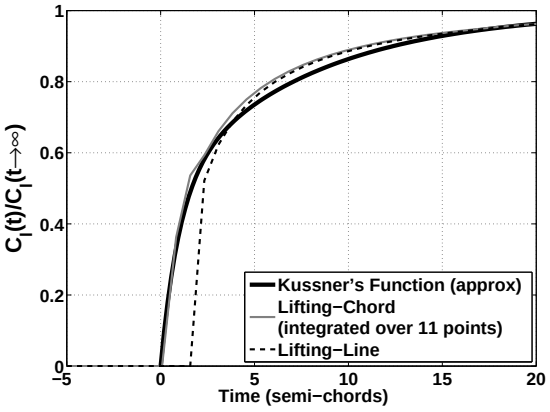

Figure 2: *Analytical and numerical solutions to Küssner's problem compared. (The leading edge of the aerofoil encounters the gust at time $t = 0$).*

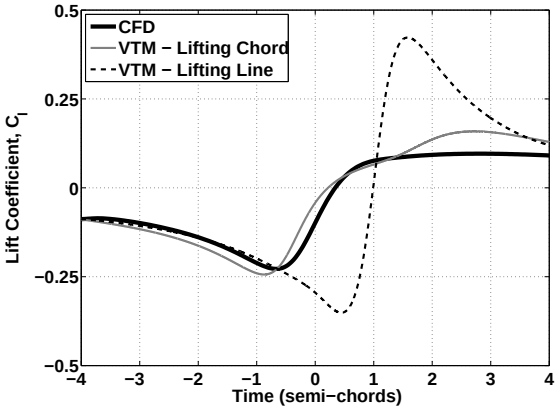

Figure 3: *Predicted aerodynamic response of an aerofoil to interaction with an isolated vortex (The vortex passes below the quarter chord of the aerofoil at time $t = 0$).*

vecting downstream at a Mach number of 0.626. The core radius of the interacting vortex is 0.162 chords (i.e. c/6.172), thus yielding a BVI of comparable dimensions to those encountered in the context of the numerical simulations[†] of the HART II system described later in this paper. This case allows the ability of each of the blade models to reproduce the highly impulsive airloads that are characteristic of blade vortex interactions to be examined in a more realistic context than that presented in the previous two sections of this paper. In the figure, the predictions of the lifting-line and lifting-chord models are compared to the predictions of a conventional CFD method (Ref. 20) which uses a pressure-velocity formulation of the Euler equations throughout the computational domain surrounding the aerofoil. The lifting-line model responds much later to the vortex-induced flow field than does the lifting-chord model, and, in comparison, over-predicts significantly the maximum loading on the aerofoil that results from the interaction. Indeed, the loading on the aerofoil once the vortex has passed downstream of the aerofoil is far better predicted by the lifting-chord model than the lifting-line model, indicating a significantly better match between the circulation that is generated on the blade using this model and the vorticity that is shed into the wake downstream of the trailing edge of the aerofoil. The consequences of this observation for the accuracy of the prediction, not only of the BVI-induced airloads on the rotor but also of the subsequent structure of the wake, are explored later in this paper.

HART II airload prediction

The results of VTM calculations at three different spatial and temporal resolutions (as summarised in Table 1) were compared to expose the effect of grid resolution on the ability of each of the blade models to predict the blade airloads for the HART II baseline case. Throughout, the structural dynamics of the blades were prescribed using six interpolation functions in the radial direction and nine in the azimuthal direction. In all cases, forty panels in a cosine distribution were used to resolve the spanwise variation in loading along the length of the blade. The rotor was trimmed to the experimental thrust coefficient and to zero aerodynamic pitch and roll moments about its hub.

During the HART II test programme, the sectional airload, C_N, at 87% of the blade span was estimated by conditionally averaging the signal from a set of pressure transducers mounted at this section of the blade. Figures 4(a) and 4(b) compare the measured blade airload at this radial station, expressed in terms of non-dimensionalised normal force coefficient ($C_N M^2$), to the airload predicted by the VTM for each of the three different resolutions of the flow field defined in Table 1. Figures 4(c) and 4(d) show the data after filtering at 10/rev to separate the signal into the low-frequency component that is associated primarily with control input and structural deformation of the blades. Parts 4(e) and 4(f) show the remaining high-frequency component of the loading that is almost exclusively associated with blade vortex interactions. These data are reproduced with magnified scale in Fig. 5.

Table 1: Computational Resolution

	size of smallest cells		timesteps per rotor revolution	degrees per timestep
coarse	R/55.5	c/3.36	350	1.03°
medium	R/83.3	c/5.04	525	0.69°
fine	R/125.0	c/7.56	800	0.45°

The major differences between the experimental data and the numerically predicted lift for the low-frequency component of the signal lie mainly to the advancing side of the disc between 0° and 120° azimuth. These differences are similar regardless of computational resolution and also irrespective of the model that is used to represent the aerodynamics of the blade. It is most likely however that the observed differences between experiment and the computational predictions of the low-frequency component of the loading on the blade can be attributed simply to errors in the interpolation that was used to prescribe the blade dynamics within the simulation. Indeed, it is suggestive that the most significant gaps in the experimental data for the structural deformation of the blades coincide rather closely with those regions of the advancing side of the rotor where the loading on the blade is least accurately predicted.

The largest differences between the two different blade aerodynamic models are to be found in their predictions of the higher harmonic, BVI-induced loading on the rotor. On the advancing side of the disc, all of the BVI events that are present in the experimental data are captured by the VTM, irrespective of the blade aerodynamic model that was used, albeit with some error in both phasing and amplitude. Changing the computational resolution has a strong effect on both the phase and the amplitude of the predicted loading fluctuations when the lifting-line model is used. In contrast, the quality of the prediction

[†] as distinct from the physical core size which is much smaller. (Ref. 9)

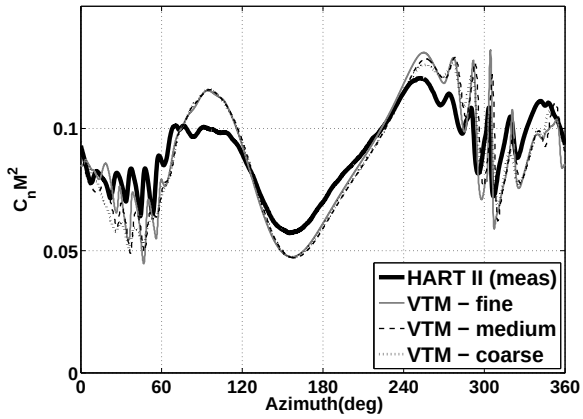

(a) *Lifting-line model - Full signal*

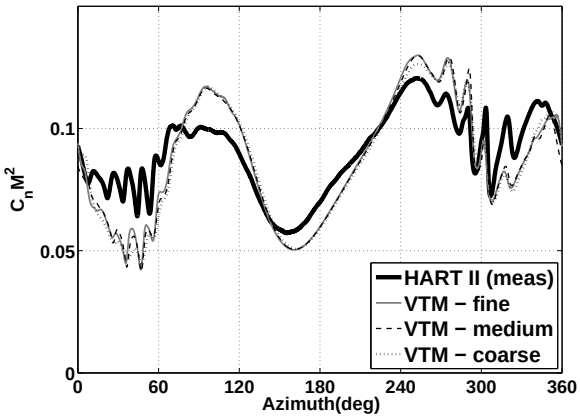

(b) *Lifting-chord model - Full signal*

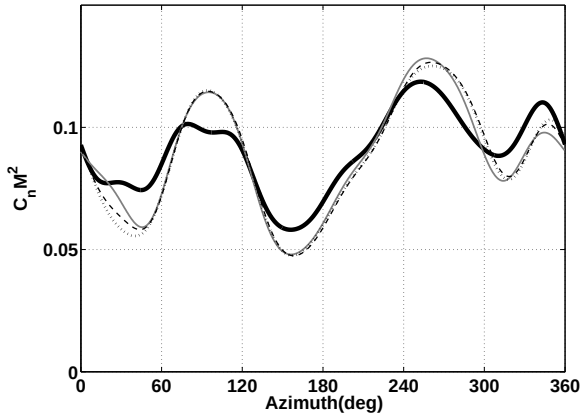

(c) *Lifting-line model - Signal filtered to include only the lower harmonic components (0-10 per rotor revolution)*

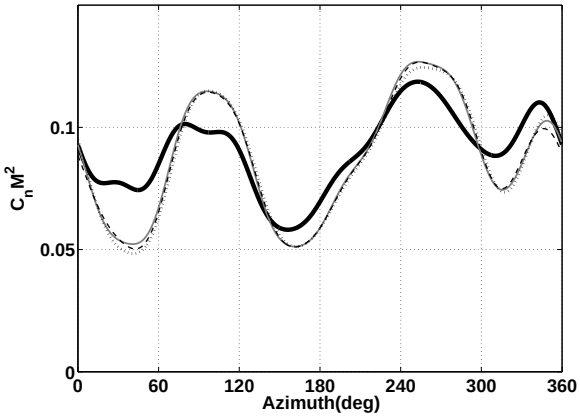

(d) *Lifting-chord model - Signal filtered to include only the lower harmonic components (0-10 per rotor revolution)*

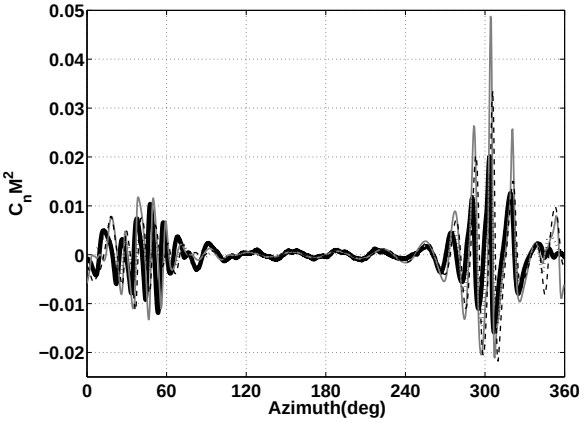

(e) *Lifting-line model - Signal filtered to include only the higher harmonic components (greater than 10 per rotor revolution)*

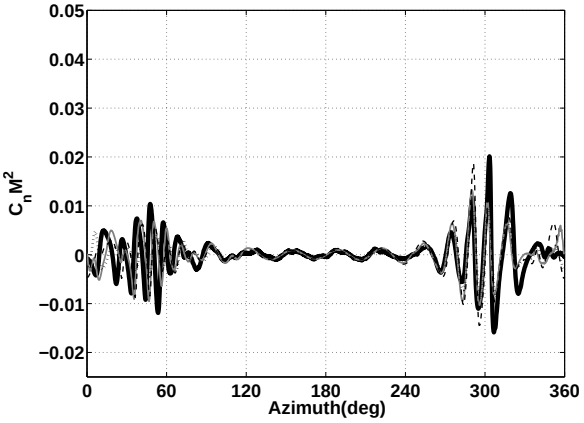

(f) *Lifting-chord model - Signal filtered to include only the higher harmonic components (greater than 10 per rotor revolution)*

Figure 4: *Comparison of blade loading ($C_N M^2$) at 87% span, as predicted using lifting-line and lifting-chord representations of the blade aerodynamics, against experimental data for the HART II baseline case.*

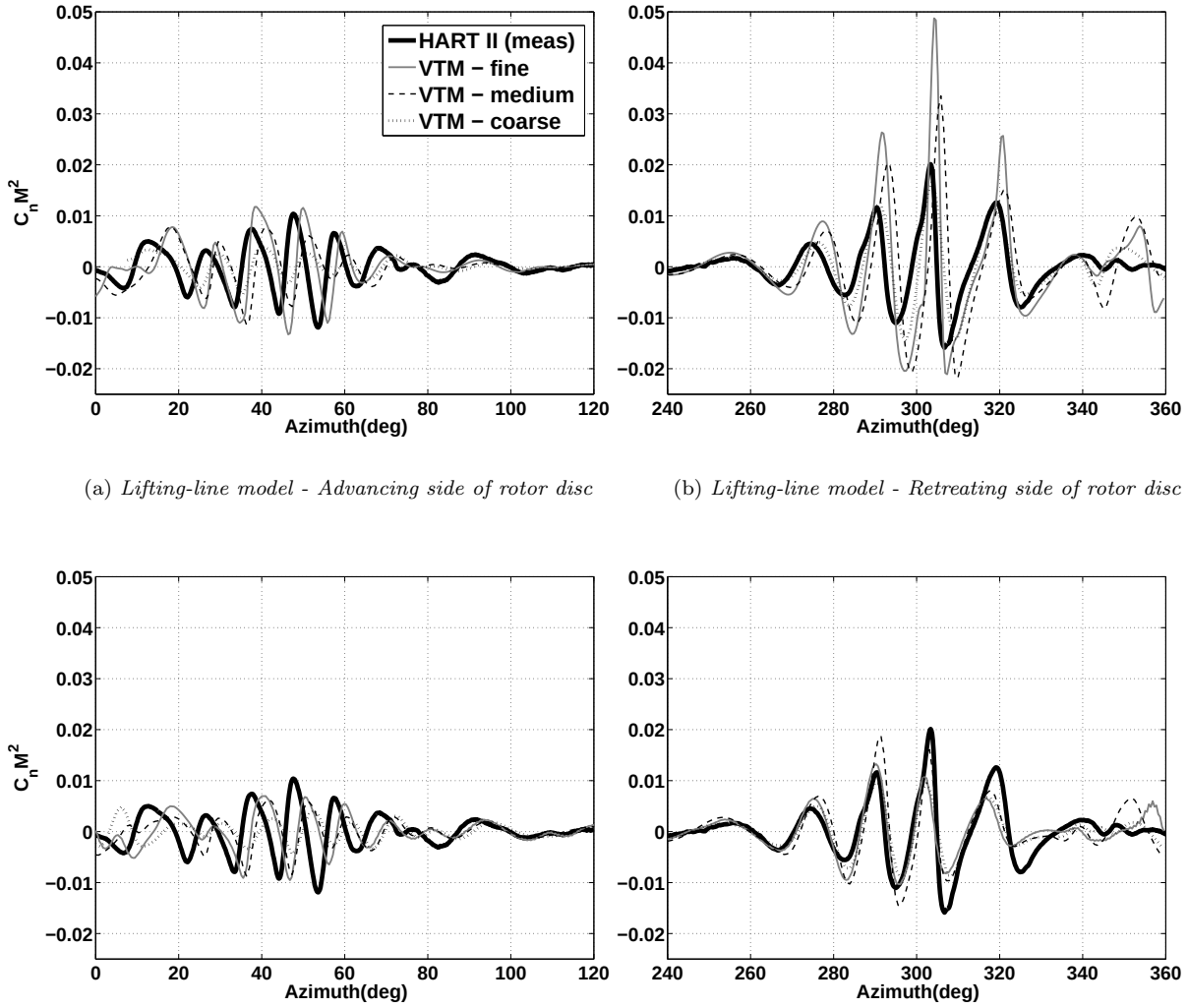

(a) *Lifting-line model - Advancing side of rotor disc*

(b) *Lifting-line model - Retreating side of rotor disc*

(c) *Lifting-chord model - Advancing side of rotor disc*

(d) *Lifting-chord model - Retreating side of rotor disc*

Figure 5: *Comparison of blade loading ($C_N M^2$) at 87% span, as predicted using lifting-line and lifting-chord representations of the blade aerodynamics, against experimental data for the HART II Baseline case, signal filtered to include only higher harmonic components (>10th harmonic).*

that is obtained when using the lifting-chord model is markedly insensitive to the resolution of the computation. Indeed, when the lifting-chord model for the blade aerodynamics is used, the phasing and impulse width of the individual BVI events compares very favourably with the experimental data, with only a very minor sensitivity to cell size compared to the predictions of the lifting-line model.

The differences in the grid-sensitivity of the two blade aerodynamic models are most obvious in their prediction of the BVI-induced loading on the retreating side of the disc. As the grid resolution is increased, the amplitudes of the peaks in the BVI-induced loading on the blade that are predicted by the lifting-line model increase markedly, resulting in a gross misrepresentation of the experimental data at the finest computational resolution. This behaviour can be understood fairly readily. The VTM is known to preserve very accurately the circulation in the flow field (Ref. 9) but, as the grid is refined, the vorticity that is associated with any particular vortex is confined to fewer cells. This results in a velocity profile for the vortex that becomes more spiky the smaller the computational cells that are used to resolve the flow. The lifting-line model, with its single-point boundary condition, is overly sensitive to the maxima and minima within the velocity field that is encountered by the blade. Indeed, as mentioned earlier, it can be

argued that the lifting-line approach fundamentally mis-represents the BVI-induced blade airloads on the rotor when, as is typically the case during a rotor BVI, the interacting vortices have core sizes that are significantly smaller than the blade chord. In contrast, the lifting-chord model, forced as it is by the (weighted) integral of the velocity along the entire chord of the blade, is much less responsive to the detail contained within the velocity field and is instead more heavily influenced by the invariant, integral properties of the flow field such as its circulation. This property of the lifting-chord model offers indeed the enticing possibility of true numerical convergence of predictions of the BVI-induced loading on the rotor as the resolution of the computational grid is increased.

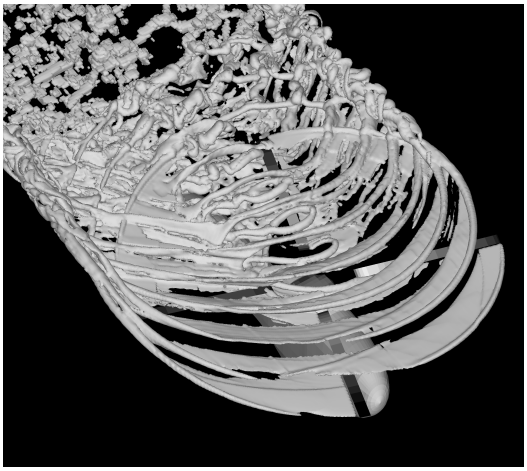

Figure 6: *Visualisation of the wake geometry of the Baseline HART II case as predicted by the VTM.*

Wake geometry

The geometry of the VTM-predicted wake of the HART II system is visualised in Fig. 6 by plotting a surface in the flow on which the vorticity has constant magnitude. This figure illustrates well the characteristic behaviour of the VTM, regardless of the model used for the aerodynamics of the rotor blade, in retaining the spatial compactness of the vortical structures that are present in the flow even after numerous rotor revolutions have elapsed.

To demonstrate the ability of the method to resolve accurately the details of the wake, and, in particular, the trajectories of the individual tip vortices as they are convected back and through the rotor disc, the computed wake structure is compared against measurements of the vortex core positions. The measurements were gathered using three-component Particle Image Velocimetry (3C-PIV) on a series of discrete longitudinal slices through the flow. Figures 7 and 8 compare contour plots of vorticity magnitude, as predicted using each of the two models for the aerodynamics of the blades, to the experimental data that was measured on the two longitudinal slices located at 40% and 70% of the rotor radius. To prevent the rotor blades from obscuring the images, the PIV measurements at locations in the first and third quadrants were collected with the rotor at 20° azimuth, and, at locations in the second and fourth quadrants, with the rotor at 70° azimuth. This difference accounts for the misalignment of the contours between the forward and aft sections of the rotor disc that is visible in the figures. Time lags in the data acquisition system gave an error of 3.5° in the measured azimuthal position of the rotor, but this has been accounted for in the presentation of the data. The positions of the vortex centres were estimated from the simple average of approximately 100 PIV images of size 0.45m by 0.38m (0.225R by 0.19R) as described in Ref. 21. The experimental meesurements are plotted in Figs. 7 and 8 as symbols, and are labelled with a number corresponding to the location of the PIV measurement plane. (In the right-handed hub coordinate system Z is positive upwards and X is positive aft. The rotor hub is located at the origin of the coordinate system.)

These figures illustrate the ability of the VTM to capture accurately the geometry of the rotor wake, irrespective of the method by which the blade loading is calculated and hence by which the vorticity source into the flow field is calculated. The locations of the maxima in the computed vorticity distribution in the wake show, in general, very good correlation with the experimentally measured vortex positions. This is true for both the slices close to the rotor hub and for those which lie closer to the tips of the blades. On the forward half of the rotor disc the prediction is better on the retreating side than on the advancing side of the rotor, which is consistent with the observed accuracy of the blade airload predictions, although such a trend is less obvious toward the rear of the rotor disc. Indeed, the positions of the vorticity maxima, as predicted by the VTM using both lifting-chord and lifting-line blade aerodynamic models, are all well within one chord length (c/R = 0.0605) of the experimentally measured positions of the vortex cores.

The most obvious differences between the two different models for the loading on the blades is how they represent the structural features of the tip vortex when resolved on the observation planes at Position 1 in Fig. 7 and Position 17 in Fig. 8, in other words when the vortex is relatively young. In both cases, the lifting chord model predicts more accurately the position of the young tip vortex by capturing more accurately the slight curvature to the inboard sheet of vorticity as it rolls up just downstream of the advancing blade.

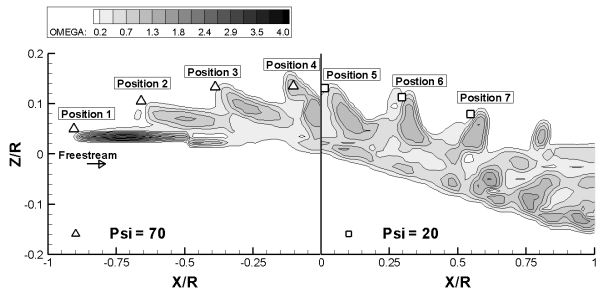

(a) *Lifting-line model - Advancing side of the rotor disc*

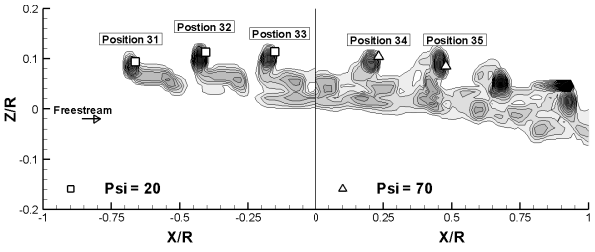

(b) *Lifting-line model - Retreating side of the rotor disc*

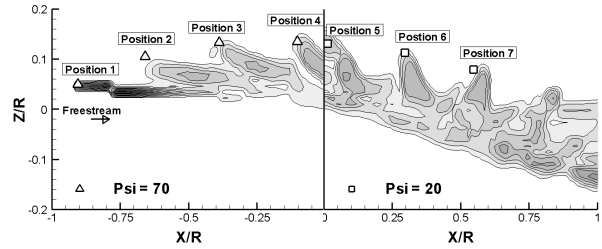

(c) *Lifting-chord model - Advancing side of the rotor disc*

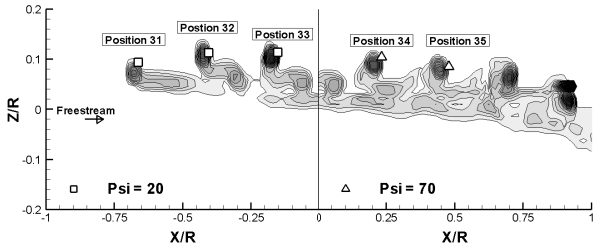

(d) *Lifting-chord model - Retreating side of the rotor disc*

Figure 7: *Computed wake structure (contours of vorticity magnitude) and measured vortex core positions (symbols) compared on a longitudinal slice through the wake at 40% of the rotor radius.*

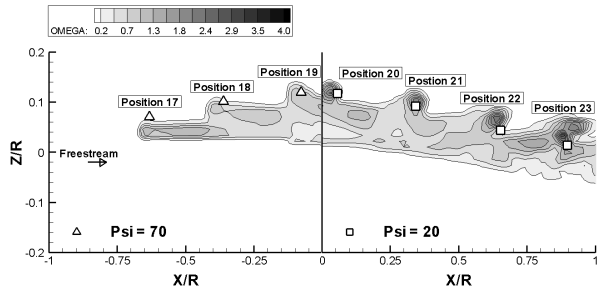

(a) *Lifting-line model - Advancing side of the rotor disc*

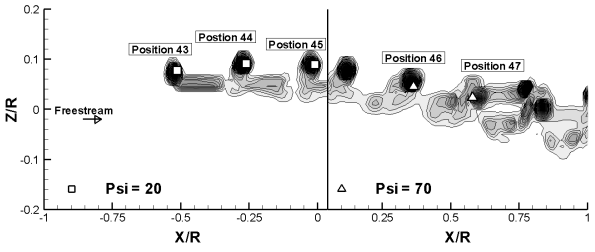

(b) *Lifting-line model - Retreating side of the rotor disc*

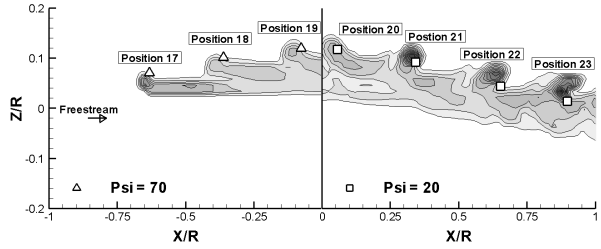

(c) *Lifting-chord model - Advancing side of the rotor disc*

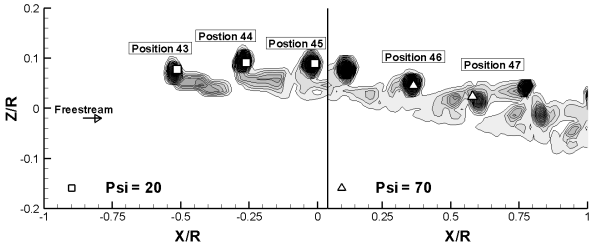

(d) *Lifting-chord model - Retreating side of the rotor disc*

Figure 8: *Computed wake structure (contours of vorticity magnitude) and measured vortex core positions (symbols) compared on a longitudinal slice through the wake at 70% of the rotor radius.*

The formation of the blade-tip vortices of the HART II rotor is known to be an extremely complex process. The flight condition of the baseline HART II case, combined with the twist distribution on the blades, results in a very flat loading profile along the span of the blade as it traverses the advancing side of the rotor. The vorticity that is deposited into the flow immediately behind the trailing edge of the blade thus forms a broad sheet, with relatively weak but uniform strength across its width, rather than a concentrated vortex. This sheet of vorticity then takes some time to roll up, forming a compact tip vortex only after about one quarter of a revolution of the rotor has elapsed.

During the HART II experiment, a series of very detailed flow measurements were gathered using a high-resolution 3C-PIV method to track the evolution of the vortex near the tips of the blades on the advancing side of the rotor. This data can be exploited very effectively to address the question of how well the very fine-scale processes that occur within the wake of the rotor are represented within the VTM, and how these are affected by the fidelity of the model for the aerodynamics of the blades. One such PIV measurement, captured on the observation plane just behind the advancing blade (plane 17), is depicted in Fig. 9.

The vorticity component normal to the measurement plane was extracted from the numerical data by suitable interrogation of the three-dimensional vorticity field surrounding the rotor, and was estimated from the experimental PIV data by numerical differentiation of the measured velocity field. The experimental data plotted here is the simple average of approximately 100 PIV images. This results in some smearing of the detailed vortex properties giving a mis-representation of the size of core radius and the maximum circulation but correctly detailing the mean position of the vortex core. The grid-lines on the plots of predicted vorticity distribution coincide with the boundaries of the computational cells[‡]. The experimental measurements show the beginnings of a concentrated tip vortex just outboard of a well-defined inboard wake sheet. Qualitatively, the structure of the measured vorticity distribution is very well captured by the VTM using either blade model. Interestingly though, the slight curvature of the inboard sheet of vorticity, that at this position is well captured by the lifting-chord aerodynamic model, is missed entirely by the VTM when the lifting-line model is used to generate the source of vorticity from the blade into the flow. Moreover, the lifting-chord model more accurately reproduces the experimentally measured position of the

[‡]The unevenness of the lines is a consequence of the PIV observation planes cutting obliquely across the underlying VTM cell structure.

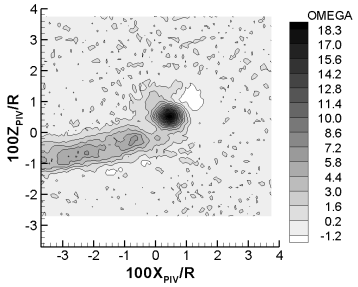

(a) *PIV high resolution data*

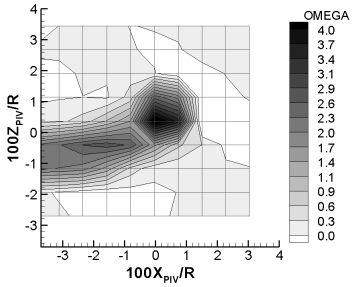

(b) *PIV resolution reduced to be comparable to numerical resolution*

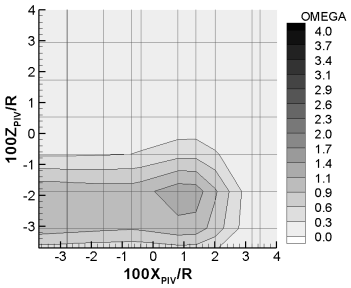

(c) *Lifting-line model - medium computational resolution*

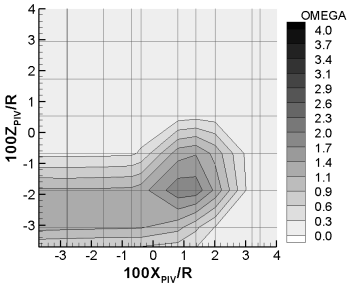

(d) *Lifting chord model - medium computational resolution*

Figure 9: *Comparison of vorticity field on the advancing side of the rotor, at a wake age of* 25.3° *(BL case, position 17)*

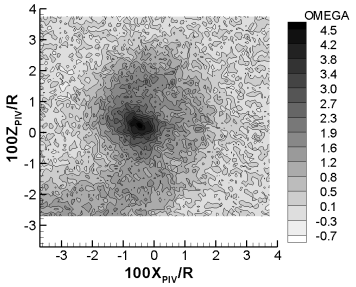

(a) *PIV high resolution data*

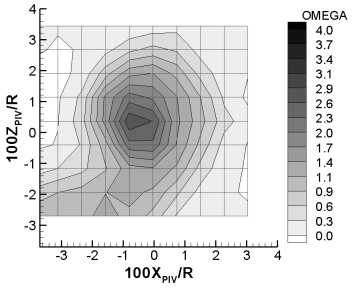

(b) *PIV resolution reduced to be comparable to numerical resolution*

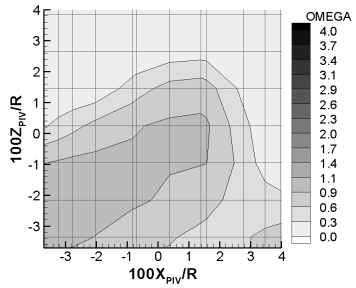

(c) *Lifting-line model - medium computational resolution*

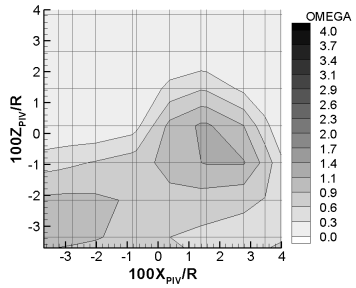

(d) *Lifting chord model - medium computational resolution*

Figure 10: *Comparison of vorticity field on the advancing side of the rotor, at a wake age of* 205.3° *(BL case, position 19)*

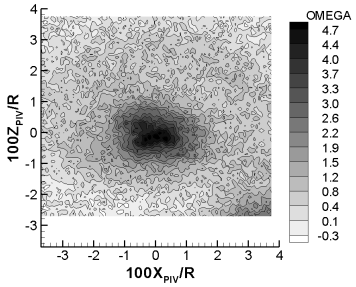

(a) *PIV high resolution data*

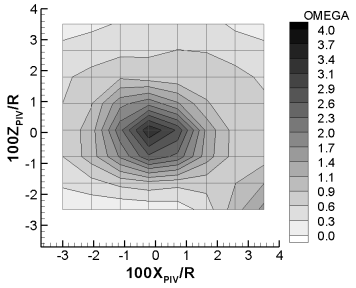

(b) *PIV resolution reduced to be comparable to numerical resolution*

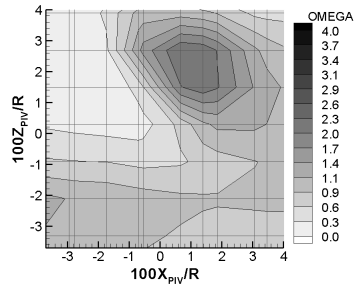

(c) *Lifting-line model - medium computational resolution*

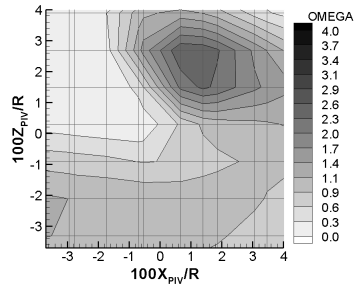

(d) *Lifting chord model - medium computational resolution*

Figure 11: *Comparison of vorticity field on the advancing side of the rotor, at a wake age of* 425.3° *(BL case, position 22)*

vortex core on this observation plane than does the lifting-line model.

In an earlier study of the wake system of the HART II rotor by Kelly and Brown (Ref. 9) it was argued that the subtlety of the features that can be resolved by the VTM, for example the slight curvature of the inboard sheet, was perhaps limited by the rectangular topology of the underlying discretisation of the computational domain. In the light of the results presented here, where a similar grid discretisation has been used for each blade model, it can be argued instead that the VTM is perhaps more sensitive than previously thought to small differences in the distribution of vorticity as it is sourced from the blades into the flow field.

A number of similar measurements were taken on observation planes further downstream to allow the structure of the tip vortex to be investigated well after the initial rollup process had run to completion. Figures 10 and 11 present the wake structure at a significantly later age than in Fig. 9 (at 205.3° and 425.3° wake age, i.e. on PIV planes 19 and 22) once the vortex sheet behind the rotor blade has almost entirely concentrated into a coherent tip vortex. These figures show again the very good qualitative agreement between predictions and the measured shape and size of the tip vortex and inboard sheet as this structure evolves to form a coherent, isolated vortex. Once again the arc-like vortical features within the vorticity distribution on the observation plane at position 19 are more accurately captured by the lifting-chord model than by the lifting-line approach. As is to be expected though, the choice of model for the aerodynamics of the rotor blades has little or no effect on the positions of the vortex cores further downstream, or indeed on the detailed structure of the flow once the vortices have aged considerably. This is illustrated in Fig. 11 where qualitatively there is little difference in the flow fields that are produced by the two different blade models far downstream of the generating blade.

Conclusion

The effect of the fidelity of the blade aerodynamic model on the prediction of the high-frequency airloads that are associated with blade vortex interactions has been assessed by coupling the Vorticity Transport Model (VTM) to two different models for the aerodynamics of the blade. The first model is an extension of the Weissinger-L lifting-line model, in which the strength of a bound vortex, placed at the quarter-chord of each blade panel, is determined by imposing a zero-through flow boundary condition at a single point located at the three-quarter chord of the panel. This approach is compared to a second, 'lifting-chord' method that is based on classical unsteady thin aerofoil theory. In this approach, the aerodynamic environment of the blade is represented by a series of weighted integrals over the chord of each blade panel.

In contrast to the lifting-line model, the lifting-chord model has been shown to distinguish accurately between those effects on the blade airloads which are due to a sudden change in angle of attack and those which are due to penetration of a vertical gust. The lifting-chord approach also more accurately represents the unsteady lift, in terms of both phase and amplitude, that is generated by an aerofoil in response to an encounter with an isolated, freely convecting vortex.

Predictions of blade airloads and wake structure, obtained using the VTM in conjunction with each of the blade aerodynamic models, have been compared against data gathered during the HART II experimental programme. The rotor was flown in a descending flight condition in which the loading on its blades contained significant high-frequency content due to the presence of blade vortex interactions. This data has been used in the present paper to analyse the ability of each of the blade aerodynamic models to capture the detailed, high frequency, BVI-induced loading on the rotor. The dynamics of the blades were prescribed to follow the experimentally-measured blade motion, thus allowing any effects on the quality of the simulation that are due to structural deformations of the rotor blades to be separated from those that are induced by the aerodynamics of the system.

The quality of the prediction of the low-frequency component of the blade loading is negligibly influenced by the model that is used to represent the aerodynamics of the rotor blades. It is likely the the main discrepancies in the prediction of this component of the airload are simply due to a misrepresentation of the blade dynamics and are thus unrelated to the aerodynamic modelling of the system.

Where the lifting-line model was used to represent the aerodynamics of the blades, the predicted high-frequency, BVI-induced component of the loading is found to be extremely sensitive to the cell size that is used in the computations. Although the phase and impulse width is only marginally influenced, the predicted amplitude of the BVI-induced features in the loading on the blades increases significantly as the cell size that is used to resolve the wake is reduced. Indeed, as the computational resolution is increased, the calculation over-predicts significantly the amplitude of the BVI-induced features in the loading, particularly on the retreating side of the rotor. These observations confirm that deficiencies in prediction of the BVI-induced airloads that were observed in earlier work were not due simply to under-resolution of the flow field, but were also due to a mis-representation of

the aerodynamic response of the blade when subjected to the very localised perturbations in its aerodynamic environment that are characteristic of helicopter blade vortex interactions.

A marked improvement in the accuracy of the predicted high-frequency airloads of the HART II rotor is obtained when a lifting chord model for the blade aerodynamics is used instead of the lifting-line type approach. Errors in the amplitude and phase of the BVI-loading peaks are reduced and the quality of the prediction is affected to a lesser extent by the computational resolution. In particular, the over-prediction of the amplitude of the BVI events, which occurs on the retreating side of the disc as the resolution of the computation is increased when using the lifting-line model, is avoided. The insensitivity of the lifting-chord model to the resolution of the computation can be explained in terms of its reduced sensitivity to the localised, small-scale features of the flow field and the dependence of its predictions rather on the integral, invariant properties of the flow field. In the context of helicopter BVI, the primary advantage of this approach would appear to be thus the possibility that it offers of true numerical convergence of predictions as the resolution of the computational grid is increased.

VTM predictions of the geometry of the wake are shown to match very closely the experimental data, no matter which method is used to represent the aerodynamics of the rotor blades. The predicted positions of the vortex cores on two longitudinal slices through the flow, one situated close to the rotor hub and further outboard along the blade span agree with the measured data to within a fraction of the blade chord. Qualitative analysis of the evolution of the tip vortex on the advancing side of the rotor shows the formation of a coherent tip vortex from the extended sheet of vorticity immediately behind the blade to be captured rather well. The slight curvature of the sheet of vorticity behind the trailing edge of the blade is captured more accurately by the lifting-chord approach than by the lifting-line approach. The positions of the youngest vortex cores on the forward half of the advancing side of the disc are thus also more accurately determined by this method. As is to be expected, the aerodynamic model has much less effect on the predicted vortex positions as the wake increases in age.

Acknowledgements

The authors would like to thank the members of the HART team for providing the data that was used in this study. In particular, the authors would like to thank Berend van der Wall and Joon Lim for their useful comments during the course of the research leading to this paper.

References

1. van der Wall, B. G., Junker, B., Burley, C., Brooks, T., Yu, Y., Tung, C., Raffel, M., Richard, H., Wagner, W., Mercker, E., Pengel, K., Holthusen, H., Beaumier, P., and Delrieux, Y., "The HART II test in the LLF of the DNW - a Major Step towards Rotor Wake Understanding," *Proceedings of the 28th European Rotorcraft Forum*, Bristol, England, 2002.

2. van der Wall, B. G., Burley, C., Yu, Y., Richard, H., Pengel, K., and Beaumier, P., "The HART II test–Measurement of helicopter rotor wakes," *Aerospace Science and Technology*, Vol. 8, No. 4, 2004, pp. 273–284.

3. Lim, J., Tung, C., Yu, Y., Burley, C., Brooks, T., Boyd, D., van der Wall, B. G., Schneider, O., Richard, H., Raffel, M., Beaumier, P., Delrieux, Y., Pengel, K., and Mercker, E., "HART II: Prediction of Blade-Vortex Interaction Loading," *Proceedings of the 29th European Rotorcraft Forum*, Friedrichshafen, Germany, 2003.

4. Yu, Y., Tung, C., van der Wall, B. G., Pausder, H., Burley, C., Brooks, T., Beaumier, P., Delrieux, Y., Mercker, E., and Pengel, K., "The HART-II Test: Rotor Wakes and Aeroacoustics with Higher-Harmonic Pitch Control (HHC) Inputs – The Joint German/French/Dutch/US Project," *Proceedings of the American Helicopter Society 58th Annual Forum*, Montreal, Canada, 2002.

5. Lim, J., Nygaard, T., Strawn, R., and Potsdam, M., "BVI airloads prediction using CFD/CSD loose coupling," *Proceedings of the American Helicopter Society Annual Forum, Vertical Lift Design Conference*, Vol. , 2006, pp. 229–242.

6. J. W. Lim and R. C. Strawn, "Prediction of HART II Rotor BVI Loading and Wake System Using CFD/CSD Loose Coupling," *Proceedings of the 45th AIAA Aerospace Sciences Meeting and Exhibit*, Paper AIAA-2007-1281, Reno, Nevada, USA, Jan 2007.

7. Whitehouse, G., Boschitsch, A., Quackenbush, T., Wachspress, D., and Brown, R. E., "Novel Eulerian Vorticity Transport Wake Module for Rotorcraft Flow Analysis," *Proceedings of the American Helicopter Society 63rd Annual Forum*, Virginia Beach, USA, 2007.

8. Kelly, M., Duraisamy, K., and Brown, R. E., "Predicting Blade Vortex Interaction, Airloads and Acoustics using the Vorticity Transport Model," *Proceedings of the American Helicopter Society 9th Aeromechanics Specialist Meeting*, San Francisco, USA, 2008.

9. M. E. Kelly and R. E. Brown, "Predicting the wake structure of the HART II rotor using the Vorticity Transport Model," *Proceedings of the European Rotorcraft Forum*, Liverpool, UK, 2008.

10. Peters, D., Hsieh, M.-C., and Torrero, A., "A state-space airloads theory for flexible airfoils," *Journal of the American Helicopter Society*, Vol. 52, No. 4, 2007, pp. 318–328.

11. Brown, R. E. and Line, A., "Efficient High-Resolution Wake Modelling using the Vorticity Transport Model," *AIAA Journal*, Vol. 43, No. 7, 2005, pp. 1434–1443.

12. R. E. Brown, "Rotor Wake Modeling for Flight Dynamic Simulation of Helicopters," *AIAA Journal*, Vol. 38, No. 1, 2000, pp. 57–63.

13. E. F. Toro, "A Weighted Average Flux Method for Hyperbolic Conservation Laws," *Proceedings of the Royal Society of London, Series A: Mathematical and Physical Sciences*, Vol. 423, 1989, pp. 401–418.

14. Kenyon, A. R. and Brown, R. E., "Wake Dynamics and Rotor-Fuselage Aerodynamic Interactions ," *Journal of the American Helicopter Society*, Vol. 54, No. 1, 2009.

15. O. Schneider, "Analysis of SPR measurements from HART II," *Aerospace Science and Technology*, Vol. 9, No. 5, 2005, pp. 409–420.

16. Schneider, O., van der Wall, B. G., and Pengel, K., "HART II Blade Motion Measured by Stereo Pattern Recognition (SPR)," *Proceedings of the American Helicopter Society 59th Annual Forum*, Phoenix, Arizona, 2003.

17. Pengel, K., Müller, R., and van der Wall, B. G., "Stereo Pattern Recognition – the technique for reliable rotor blade deformation and twist measurement," *Proceedings of the American Helicopter Society International Meeting on Advanced Rotorcraft Technology and Life Saving Activities (Heli Japan)*, Tochigi, Utsunomiya, Japan, 2002.

18. H. Wagner, "Über die Entstehung des dynamischen Auftriebes von Tragflügeln," *Zeitschift für Angewandte Mathematik und Mechanik*, Vol. 5, No. 1, 1925, pp. 17–35.

19. H. G. Küssner, "Zusammenfassender Bericht über den instationären Auftrieb von Flügeln," *Luftfahrt-Forschung*, Vol. 13, No. 12, 1936, pp. 410–424.

20. Duraisamy, K. and Brown, R. E., "Aerodynamic Response of a Hovering Rotor to Ramp Changes in Pitch Input," *Proceedings of the American Helicopter Society 64th Annual Forum*, Montreal, Canada, 2008.

21. van der Wall, B. G. and Richard, H., "Analysis Methodology for 3C PIV Data of Rotary Wing Vortices," *Experiments in Fluids*, Vol. 40, No. 4, 2006, pp. 798–812.